A Unified Approach to Noise Removal, Image Enhancement, and Shape Recovery*†

R. Malladi‡ and J. A. Sethian

Department of Mathematics
and
Lawrence Berkeley National Laboratory
University of California, Berkeley, CA 94720
e-mail: {malladi,sethian}@math.berkeley.edu

December 17, 1999

Abstract

We present a unified approach to noise removal, image enhancement, and shape recovery in images. The underlying approach relies on the level set formulation of curve and surface motion, which leads to a class of PDE-based algorithms. Beginning with an image, the first stage of this approach removes noise and enchances the image by evolving the image under flow controlled by min/max curvature flow and by the mean curvature. This stage is applicable to both salt-and-pepper grey-scale noise and full-image continuous noise present in black and white images, grey-scale images, texture images and color images. The noise removal/enhancement schemes applied in this stage contains only one enhancement parameter, which in most cases is automatically chosen, and stop automatically at some optimal point. Continued application of the scheme produces no further change. The second stage of our approach is the shape recovery of a desired object; we again exploit the level set approach to evolve an initial curve/surface towards the desired boundary, driven by an image-dependent speed function which automatically stops at the desired boundary.

EDICS number IP 1.9

Permission to publish this abstract separately is granted.

*Correction citation: Malladi, R., and Sethian, J.A., IEEE Transactions on Image Processing, 5, 11, pp. 1154-1168, 1996.

†Supported in part by the Applied Mathematics Subprogram of the Office of Energy Research under DE-AC03-76SF00098, and the National Science Foundation DARPA under grant DMS-8919074.

‡NSF Postdoctoral Fellow in Computational Science and Engineering

1 Introduction

In this paper, we present a unified approach to noise removal, image enhancement, and shape recovery in images. The fundamental link is the level set formulation of propagating interfaces, which is a mathematical formulation and numerical algorithm for tracking the motion of curves and surfaces. In the work presented here, this formulation leads to a class of PDE-based algorithms which are image-dependent and contain user-controlled scale-dependent properties. These partial differential equations are used in two stages, first, to remove noise and enhance images, and second, to recover shapes in the processed image.

In Stage I, given an image, we remove noise and enhance the image by evolving the under flow controlled by min/max curvature flow. Briefly, the min/max approach evolves equal image intensity contours in their normal directions under a flow that depends on their local curvature and on background information extracted from the underlying domain; this approach is described in some detail in Section III. The key to this approach rests on a min/max switch function that determines the appropriate motion. Our min/max flow has the following characteristics:

1. The min/max flow removes small-scale noise by selecting the correct evolution equation.
2. The larger, global properties of shapes in the image field are maintained.
3. Furthermore, and equally importantly, the flow stops once this noise is removed: Continued application of the scheme produces no further change.
4. Edge definition is maintained, and, in some global sense, area inside boundaries is preserved.
5. The noise removal capabilities of the min/max flow is scale-dependent, and can hierarchically adjusted.
6. The scheme requires only a nearest neighbor stencil evaluation.

A variation on our basic scheme, relying on evaluations of mean curvature and associated evolution equations can be used to selectively enhance different aspects of the image, and is useful when a particular type of noise removal/enhancement is desired. Our approach is applicable to both salt-and-pepper grey-scale noise and full-image continuous noise present in black and white images, grey-scale images, texture images and color images.

In Stage II of the process, we recover objects from the processed image. The goal here is to fit a boundary to match the shape of the desired object. Our approach works by evolving an initial front using the level set methodology of propagating interfaces, with a speed function synthesized from the image. This speed function is constructed so that it forces the evolving boundary to stop at the object boundary by exploiting information about the image gradient. Our level set approach to shape recovery has the following characteristics:

1. No previous information about the topology of the shape boundary is required; due to the level set formulation, the evolving shape boundary can break, change topology, and merge as it searches for the object boundary.

2. The recovery techniques are applicable to both two and three-dimensional image fields.

3. In areas away from the boundary, the front evolves extremely quickly.

4. The image processing/enchancement in Stage I can be linked with with the synthesized speed function to accentuate desired object boundaries and aid in shape recovery.

In this paper, we present a collection of results to demonstrate the features of this system. We begin by applying our min/max scheme for noise removal and enhancement to a variety of black and white, and grey scale images. We then follow with shape recovery of objects from within enchanced images. We then put the entire sequence together, and show enchancement, segmentation, and shape recovery of cardiac data from two and three-dimensional image fields obtained from CT, and MRI scans.

The methods presented in this paper are derived from the Osher-Sethian [28] level set formulation of front propagation, which grew out of earlier by Sethian [35] on the mathematical formulation of curve and surface motion. The design of a PDE-based approach to image enhancement and noise removal was introduced in two pivotal papers; the work of Alvarez, Lions and Morel [3] and the work of Osher-Rudin [27]. While the min/max scheme described here starts from the original curve evolution work given in [35] and proceeds along different lines, it owes a considerable debt to the above works. The application of the same level set perspective to shape recovery in Stage II was developed by Malladi, Sethian, and Vemuri in previous work; see [24, 25]. That work was motivated by the large body of work on energy minimization, see [7, 38, 39, 19, 13, 41].

To be sure, there is a wide spectrum of image processing and shape recovery algorithms in existence, some of which are briefly mentioned in the following section. This work falls under the category of partial differential equations-based schemes. In different applications and different circumstances, other schemes may be preferable. The goal of this paper is not to promote one approach in all situations, but instead to offer a cohesive approach based on a unified mathematical perspective.

The outline of this paper is as follows. In Section II, we describe background work in this area; including in particular previous work using level set techniques in this context. In Section III, we describe our min/max scheme for image enchancement and noise removal that comprises Stage I of the process. In Section IV, we describe the level set approach to shape segmentation and recovery. In Section V, we compare our min/max approach to image smoothing and enchancement with other approaches, and demonstrate the versatility of the shape recovery scheme. In Section VI, we apply the unified model for noise removal, image enchancement and shape recovery to a series of applications.

2 Background/Previous Work

2.1 Goal of Image Smoothing/Enchancement and Shape Recovery

The essential idea in image smoothing is to filter noise present in the image signal without sacrificing the useful detail. In contrast, image enhancement focuses on preferentially highlighting certain image features. The subject is vast, and we refer to the interested reader to standard works in the field, see [16, 18] and references therein. Traditionally, both 1-D and 2-D signals are smoothed by convolving them with a Gaussian kernel; the degree of blurring is controlled by the characteristic width of the Gaussian filter. Since the Gaussian kernel is an isotropic operator, it smooths across the region boundaries thereby compromising their spatial position. A variety of techniques have been introduced to improve upon this idea, including anisotropic diffusion schemes, see Perona and Malik [29], the optimal Wiener filter [14], and more recently wavelet processing [31].

Together, such noise removal/smoothing and image enchancement act as precursors to many low level vision procedures such as edge finding [26, 8], shape segmentation [19, 25, 9, 10], and shape representation [22]. Here, the goal is extract a desired shape from an image, and represent that shape in such a way that further measurement and testing can be performed. Typical techniques for finding and representing object

shapes include both passive and active models. Models of shape such as generalized cylinders, introduced by Binford [6], and lumped-parameter family of shapes such as superquadric models [5] are purely geometric, hence passive; they attempt to directly build the shape from the image gradients. Generalized cylinders are used to model elongated shapes with axial symmetry, while the superquadric shape models are well suited for object recognition tasks because one can express them compactly using a small set of parameters.

In contrast, active models work by attempting to evolve a shape until it is attracted and stabilizes at places where the image gradient changes markedly. Thus, one uses an image-based constraint function to mold the trial shape until it reconstructs the desired region. Generalized splines with elasticity constraints [7, 38, 41] are prime examples of the active shape modeling paradigm.

2.2 Level Set Methods for Image Smoothing/Enchancement and Shape Recovery

2.2.1 Level Set Methods

The Osher-Sethian level set method for propagating interfaces was introduced in [28], based on mathematical and numerical work by Sethian [35] on curve and surface motion. It offers a highly robust and accurate method for tracking interfaces moving under complex motions. Its major virtue is that it naturally construct the fundamental weak solution to surface propagation posed by Sethian [34, 35]. In standard, typical techniques, the motion of a curve or surface is represented by a discrete parameterization of the object by a set of points whose positions are updated according to a given set of evolution equations. This is a Lagrangian perspective, and is referred to by a variety of names, including snakes, string methods, and marker particles. Two central drawbacks of such techniques are that they rely on a continual reparameterization of the curve/surface as it becomes more complex, and that profound difficulties occur when the topology of the evolving shape changes.

In contrast, the level set formulation offers an alternative framework, based on the view that the moving front can be viewed as the zero level set of higher dimensional function. The evolution of this higher dimensional function resembles a Hamilton-Jacobi equation with parabolic right-hand sides. In this setting, sharp gradients and cusps can form easily, and the effects of curvature may be easily incorporated. The key numerical idea is then to borrow the technology from the numerical solution of hyperbolic conservation laws and transfer these ideas to the Hamilton-Jacobi setting, which then guarantees that the correct entropy satisfying solution will be obtained. Given complex speed functions which may depend on the local curvature,

normal direction, pure advection velocities and underlying physics, this approach has been used to study a wide variety of interface propagation problems, including the generation of minimal surfaces [11], fast interface techniques [1], character recognition [22], singularities and geodesics in moving curves and surfaces in [12], flame propagation [40, 42], grid generation [37], and semiconductor manufacturing [2].

2.2.2 Application of Level Set Methods to Image Smoothing/Enchancement and Shape Recovery

A significant advancement in image smoothing and enchancement was made by Alvarez, Lions, and Morel (ALM) [3], who presented a comprehensive model for image smoothing which includes the other models as special cases.

The ALM model consists of solving an equation of the form

$$I_t = g(|\nabla G * I|)\ \kappa\ |\nabla I|, \quad \text{with} \quad I(x, y, t = 0) = I_0(x, y), \tag{1}$$

where $G * I$ denotes the image convolved with a Gaussian filter. The geometric interpretation of the above diffusion equation is that the isointensity contours of the image move with speed $g(|\nabla G * I|)\kappa$, where $\kappa = \text{div}\frac{\nabla I}{|\nabla I|}$ is the local curvature. One variation of this scheme comes from replacing the curvature term with its affine invariant version (see Sapiro and Tannenbaum [32]). By flowing the isointensity contours normal to themselves, smoothing is performed perpendicular to edges thereby retaining edge definition. At the core of both numerical techniques is the Osher-Sethian level set algorithm for flowing the isointensity contours; this technique was also used in related work by Rudin, Osher and Fatemi [30].

Recently, a new set of level set-based smoothing and enhancement techniques were introduced by Malladi and Sethian, see [20, 21]. These techniques return to the original level set, curvature flow perspective, and design an image processing scheme which automatically chooses the correct flow equations to perform intraregion smoothing while maintaining edge definition. The key idea rests in the construction of a min/max switch which evolves equal image intensity contours in their normal directions under a flow that depends on their local curvature and on background information extracted from the underlying domain. This switch forces the flow to stop automatically once the scale-chosen level of smoothing/enhancement is achieved; the desired scale-dependence is a function of the pixel representation and can be chosen at any level of detail. The resulting technique is an automatic, extremely robust, computationally efficient, and straightforward

scheme. It is these set of schemes that are discussed in Section III, and which are used in our unified model of image smoothing/enchancement and shape recovery. Details about these schemes, and their applicability to a wide range of images, including salt-and-pepper grey scale noise, multiplicative noise and Gaussian noise applied to black and white, grey scale, textured, and color images may be found in [21].

The application of level set methods to shape recovery and reconstruction was developed in a series of papers, see [24, 25, 23]; application to shape representation and recognition may be found in [22]. It is a natural and appealing application of the level set approach, since the ability to change topology and follow intricate variations in evolution velocities are strengths of this approach. In this work, an initial shape is chosen, and a speed function is synthesized from the image in such a form that the evolving front stops at the boundary. This method has been used with considerable success, including a fast narrow band version in [25], and a version for three-dimensional shape recovery in [23]. A related effort exploiting the Osher-Sethian level set technique was given in [9] and later improved in [10].

In this work, we couple the min/max flow algorithms to level set shape recovery schemes to build a unified model for noise removal, enchancement, and shape recovery.

3 Stage I: Image Smoothing and Enchancement: The Min/Max Flow

In this section, we summarize the ideas behind and implementation of the mix/max scheme for image processing first presented in [20]. The basic idea is to solve a time-dependent partial differential equation which describes the evolution of isointensity contours, using a switch function which assesses the scale of the noise and chooses the appropriate terms in the differential equations. Complete details and extensive examples may be found in [21].

3.1 Front Propagation under Curvature

As a start, consider a closed, nonintersecting curve in the plane moving with speed $F(\kappa)$ normal to itself. More precisely, let $\gamma(0)$ be a smooth, closed initial curve in R^2, and let $\gamma(t)$ be the one-parameter family of curves generated by moving $\gamma(0)$ along its normal vector field with speed $F(\kappa)$. Here, $F(\kappa)$ is a given scalar function of the curvature κ. Thus, $n \cdot x_t = F(\kappa)$, where x is the position vector of the curve, t is time, and n is the unit normal to the curve.

The application of this problem to image processing comes from considering a very specific speed function, namely $F(\kappa) = -\kappa$, as shown in the seminal paper by Alvarez, Morel and Lions, see [3]. This case corresponds to a curve collapsing under its curvature. It can be shown that for an arbitrary smooth simple curve, (see Gage [15], Grayson [17]), such a curve collapses to a single point.

In Figure 1a, we show what happens to a double star-shaped region under this flow. We view the region between the two curves as the "inside" and follow the motion of the boundary between inside and the outside propagating in its normal direction with speed equal to the negative of the curvature. Here, we have evolved the front using the Osher-Sethian level set method, see [28]. Briefly, this technique works as follows. Given a moving closed hypersurface $\Gamma(t)$, that is, $\Gamma(t=0) : [0,\infty) \to R^N$, we wish to produce an Eulerian formulation for the motion of the hypersurface propagating along its normal direction with speed F, where F can be a function of various arguments, including the curvature, normal direction, e.t.c. The main idea is to embed this propagating interface as the zero level set of a higher dimensional function ϕ. Let $\phi(x, t=0)$, where $x \in R^N$ is defined by

$$\phi(x, t=0) = \pm d \tag{2}$$

where d is the distance from x to $\Gamma(t=0)$, and the plus (minus) sign is chosen if the point x is outside (inside) the initial hypersurface $\Gamma(t=0)$. Thus, we have an initial function $\phi(x, t=0) : R^N \to R$ with the property that

$$\Gamma(t=0) = (x|\phi(x, t=0) = 0) \tag{3}$$

It can easily be shown that the equation of motion given by

$$\phi_t + F|\nabla\phi| = 0, \tag{4}$$

$$\phi(x, t=0) \quad given \tag{5}$$

such that the evolution of the zero level set of ϕ always corresponds to the motion of the initial hypersurface under the given speed function F. This evolution equation Eqn. 5 is solved by means of difference operators on a fixed Eulerian grid. Care must be taken in the case where the speed function F contains a hyperbolic component. For details, see [28, 36].

We now modify the above flow. In order to be careful about signs, we simply note that the boundary of a disk initialized so that the inside of the disk corresponds to a negative value for the signed distance

function ϕ and a positive value for the signed distance function ϕ on the outside of the disk has a normal $\nabla\phi$ which points outwards away from the center of the disk, and a curvature defined as $\nabla \cdot \nabla\phi/|\nabla\phi|$ which is always positive on all the convex level contours. Thus, a flow under speed function $F = \kappa$ corresponds to the collapsing curvature flow, since the boundary moves in the direction of its normal with negative speed, and hence moves inwards.

We need to be further careful about signs and amend a previous definition. We shall refer to a speed function F in the context of the level set equation

$$\phi_t = F|\nabla\phi| \tag{6}$$

thus, from now on, F will give the speed of the front in a direction opposite to its normal direction. Thus, a curve collapsing under its curvature will correspond to speed $F = \kappa$. This will be our convention for the remainder of this paper.

Now, consider two flows, namely

- $F(\kappa) = \min(\kappa, 0.0)$
- $F(\kappa) = \max(\kappa, 0.0)$

The effect of flow under $F(\kappa) = \min(\kappa, 0.0)$ is to allow inward concave fingers to grow outwards, while suppressing the motion of the outward convex regions. Thus, the motion halts as soon as the convex hull is obtained. Conversely, the effect of flow under $F(\kappa) = \max(\kappa, 0.0)$ is to allow the outward regions to grow inwards while suppressing the motion of the inward concave regions. However, once the shape becomes fully convex, the curvature is always positive and thus the flow becomes the same as regular curvature flow; hence the shape collapses to a point. We can summarize by saying that, for the above choice of signs, flow under $F = \min(\kappa, 0.0)$ preserves some of the structure of the curve, while flow under $F = \max(\kappa, 0.0)$ completely diffuses away all of the information.

In Figure 1b, we show our original double curve collapsing under $F = \min(\kappa, 0.0)$; here, the outer part of the front moves to the convex hull, while the inner part collapses and disappears. The last shown state is stable. In Figure 1c, we show the same curve collapsing under $F = \max(\kappa, 0.0)$; here, the outer part of the front moves inwards while the inner part expands to its convex hull. Eventually, the two meet, and

the front disappears. Finally, in Figure 1d, we switch the roles of black and white; thus flow with speed $F = \max(\kappa, 0.0)$ corresponds to the same flow as in Figure 1b; changing the colors corresponds to change from the maximum flow to the minimum flow.

3.2 The Min/Max Switch

Our goal is to select the correct choice of flow so that curves are "smoothed", that is, so that small oscillations disappear but the essential properties of the front are maintained. We define the following speed function, introduced in [20] and refined considerably in [21]:

$$F_{\min\,/\,\max}^{Stencil=k} = \begin{cases} \min(\kappa, 0) & \text{if } Ave_{\phi(x,y)}^{R=kh} < 0 \\ \max(\kappa, 0) & \text{if } Ave_{\phi(x,y)}^{R=kh} \geq 0 \end{cases} \tag{7}$$

where $Ave_{\phi(x,y)}^{R=kh}$ is defined as the average value of ϕ in a disk of radius $R = kh$ centered around the point (x, y). Here, h is the step size of the grid. Thus, given a "StencilRadius" kh, the above yields a speed function which depends on the value of ϕ at the point (x, y), the average value of ϕ in neighborhood of a given size, and the value of the curvature of the level curve going through (x, y).

We can examine this speed function in some detail. For ease of exposition, consider a black region on a white background, chosen so that the interior has a negative value of ϕ and the exterior a positive value of ϕ.

- StencilRadius =0

  If the radius $R = 0$ ($k = 0$), then choice of $\min(\kappa, 0)$ or $\max(\kappa, 0)$ depends only the value of ϕ. All the level curves in the black region will attempt to form their convex hull, when seen from the black side, and all the level curves in the white region will attempt to form *their* convex hull. The net effect will be no motion of the zero level set itself, and the boundary will not move.

- StencilRadius=h

  If the average is taken over a stencil of radius h, then some movement of the zero level corresponding to the boundary is possible. If there are some oscillations in the front boundary on the order of one or two pixels, then it may be possible for the average value of ϕ at the point (x, y) to be of a different sign than the value at (x, y) itself. In this case, the flow will act as if it were selected from the "other

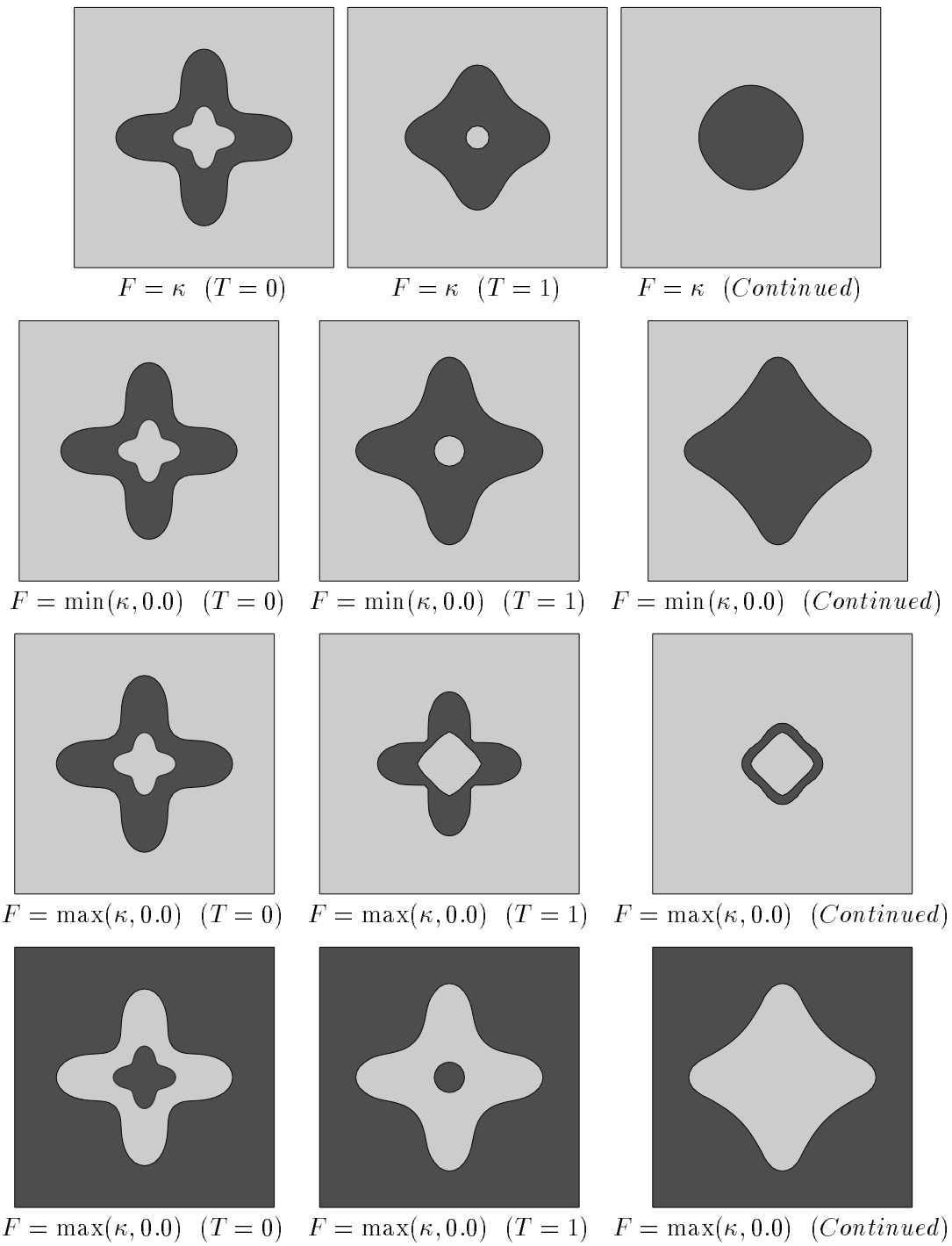

Figure 1: Motion of Complex Region under Various Flows

side", and some motion will be allowed until these first-order oscillations are removed, and a balance between the two sides is agained reached. Once this balanced is reached, no motion is possible.

- StencilRadius $=kh$

  By taking averages over a larger and larger stencil, larger amounts of smoothing are applied to the boundary; in other words, decisions about where features belong are based on larger and larger perspectives. Once features on the order of size k are removed from the boundary, balance is reached and the flow stops automatically. As an example, let $k = \infty$. Since the average will compute to a value close to the background color, on this scale all structures are insignificant, the max flow will be chosen everywhere, forcing the boundary to disappear.

We show the results of this hierarchical flows in Figure 2; we start with an initial shape in Figure 2a and first perform the min/max flow under steady-state is reached with stencil size zero in Figure 2b; in this case, no motion is possible. We then perform the min/max flow until steady-state is achieved with stencil size $k = 1$ in Figure 2c, and the continue min/max flow with a larger stencil until steady-state is again achieved in Figure 2d.

We can summarize our results as follows:

- The single min/max flow selects the correct motion to diffuse the small-scale pixel notches into the boundary.
- The larger, global properties of the shape is maintained.
- Furthermore, and equally importantly, the flow stops once these notches are diffused into the main structure.
- Edge definition is maintained, and, in some global sense, the area inside the boundary is preserved.
- The noise removal capabilities of the min/max flow is scale-dependent, and can hierarchically adjusted.
- The scheme requires only a nearest neighbor stencil evaluation.

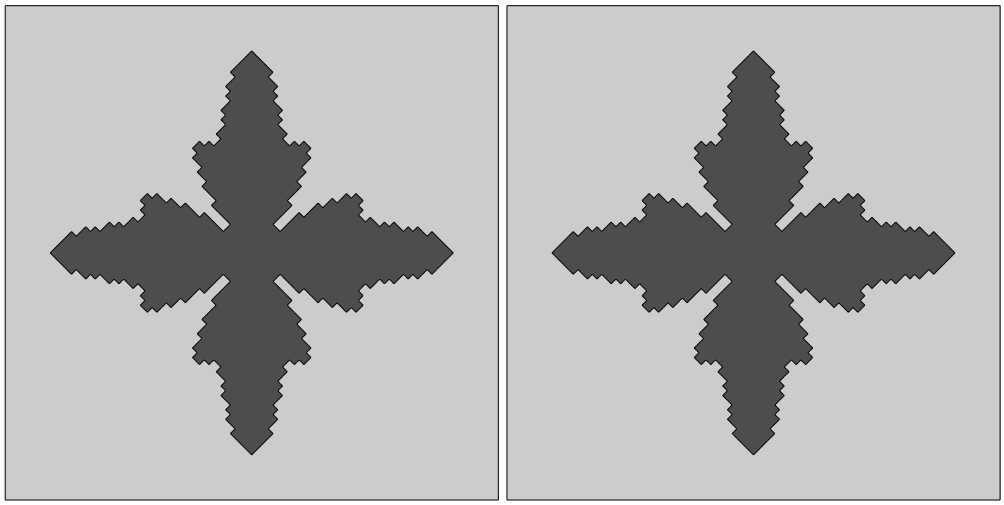

$Initial\ \ Boundary$
$\text{“}Noisy\text{”}\ \ Shape$

$Min/Max\ \ Flow:$
$Stencil\ \ Width = 0;\ \ (T = \infty)$

$Min/Max\ \ Flow:$
$Stencil\ \ Width = 1;\ \ (T = \infty)$

$Continued\ \ Min/MaxFlow:$
$Stencil\ \ Width = 2;\ \ (T = \infty)$

Figure 2: Motion of StarShaped Region with Noise under Min/Max Flow at Various Stencil Levels

The above technique applies to black and white images. An extension to grey-scale images can be easily made by replacing the fixed threshold test value of 0 with a value that depends on the local neighborhood. As designed in [20], let $T_{threshold}$ be the average value of the intensity obtained in the direction perpendicular to the gradient direction. Note that since the direction perpendicular to the gradient is tangent to the isointensity contour through (x, y), the two points used to compute are either in the same region, or the point (x, y) is an inflection point, in which the curvature is in fact zero and the min/max flow will always yield zero. By choosing a larger stencil we mean computing this tangential average over endpoints located further apart.

Formally then, our final min/max scheme, applicable to all types of images becomes:

$$F_{min/max} = \begin{cases} \max(\kappa, 0) & \text{if } Average(x, y) < T_{threshold} \\ \min(\kappa, 0) & \text{otherwise} \end{cases} \tag{8}$$

Further details about this scheme may be found in [21]. In that work, we apply these techniques to a wide range of images, including salt-and-pepper grey scale noise, multiplicative noise and Gaussian noise applied to black and white, grey scale, textured, and color images.

3.3 Examples

In this section, we provide a few examples of our min/max flow. We begin with binary images with noise. Since we are looking at black and white images, where 0 corresponds to black and 255 to white, the threshold value $T_{threshold}$ is taken as 127.5 rather than 0. In Figure 3, we add noise to a black and white image of hand-written characters. The noise is added as follows; 10% noise means that at 10% of the pixels, we replace the given value with a number chosen with uniform distribution between 0 and 255. Thus, a full spectrum of gray noise is added to the original binary image, The left column give the original figure with the corresponding percentage of noise; the right column are reconstructed values. We stress once again that the figures on the right are converged; they stop automatically, and continued application of the scheme yields no change in the results.

Next, we remove salt-and-pepper gray-scale noise from a grey-scale image. Once again, we add noise to the figure by replacing $X\%$ of the pixels with a new value, chosen from a uniform random distribution between 0 and 255, Our results are obtained as follows. We begin with two levels of noise; 25% noise in

(a) 25.0% noise

(b) Restored

(c) 50.0% noise

(d) Restored

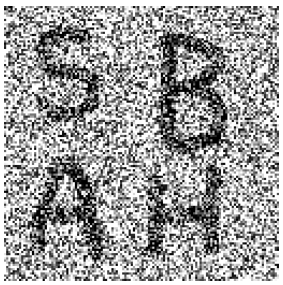

(e) 65.0% noise

(f) Restored

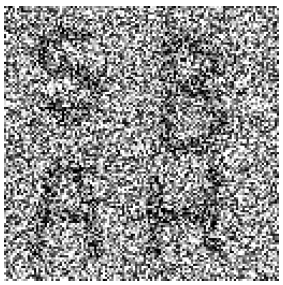

(g) 80.0% noise

(h) Restored

Figure 3: Image restoration of Binary Images with Grey-Scale Salt-and-Pepper Noise Using Min/Max Flow: Restored shapes are final shape obtained at $T = \infty$

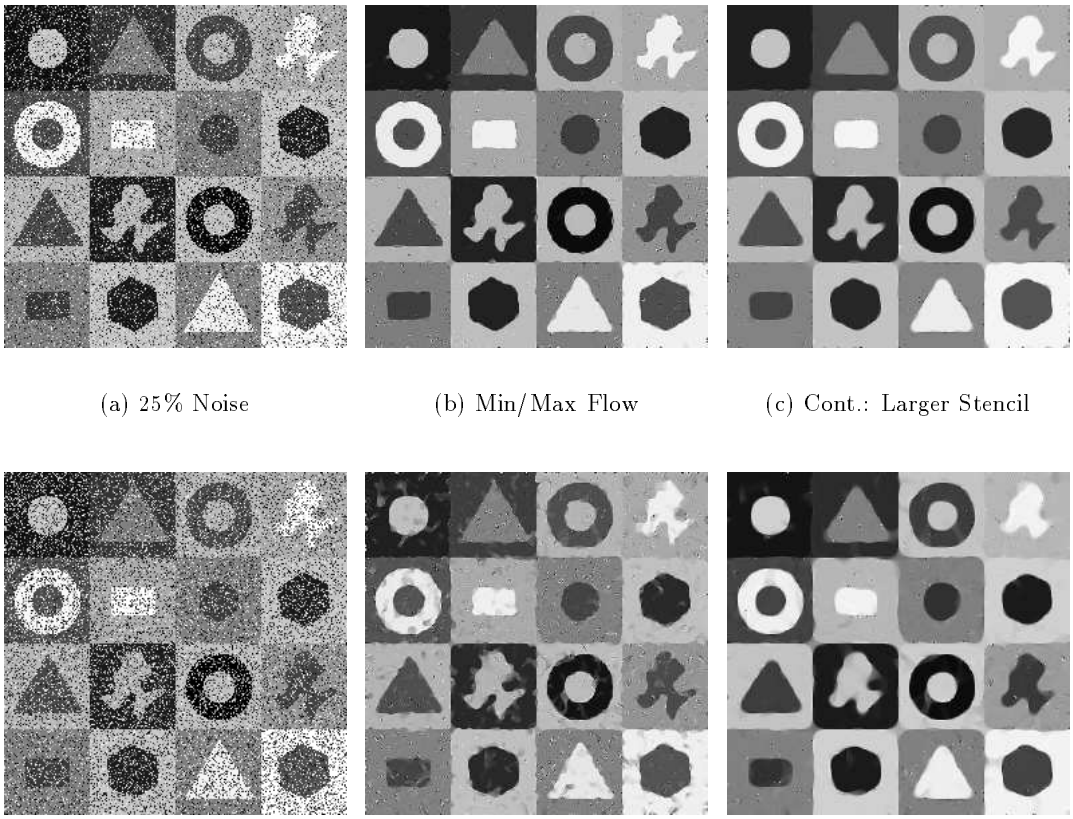

(a) 25% Noise (b) Min/Max Flow (c) Cont.: Larger Stencil

(d) 40% Noise (e) Min/Max Flow (f) Cont.: Larger Stencil

Figure 4: Min/Max Flow. The left column is the original with noise, the center column is the steady-state of min/max flow, the right column is the continuation to steady-state of the min/max flow using a larger stencil

Figure 4a and 50% noise in Figure 4d. We first use the min/max flow from Eqn.8 until a steady-state is reached in each case, (Figure 4b and Figure 4e). This removes most of the noise. We then continue with a larger stencil for the threshold to remove further noise (Figure 4c and Figure 4f). For the larger stencil, we compute the average $Average(x, y)$ over a larger disk, and compute the threshold value $T_{threshold}$ using a correspondingly longer tangent vector.

Next, we study the effect of our min/max scheme on multiplicative noise added to a grey-scale image. In Figure 5 we show the reconstruction of an image with 15% multiplicative noise.

Finally, as our last example in this section, we add 100% Gaussian grey-scale noise; that is, a random component drawn from a Gaussian distribution with mean zero is added to each (every) pixel. In Figure 6

(a) Image with Noise

(b) Min/Max:Final

Figure 5: Min/Max Flow Applied to Multiplicative Noise

we show the original with noise together with the reconstructed min/max flow image.

4 Stage II: Shape Detection and Recovery

Given an image, the goal in this section is to detect and recover the shapes of interest in such a way that the representation of those shapes is amenable to further treatment, such as in measuring changes in area, volume, e.t.c.

The level set technique for shape recovery is motivated by the active contour/snake approach to shape recovery. In order to explain the mathematics and numerics of our approach, we return to the level set equation for an interface propagating with speed F, namely

$$\phi_t + F|\nabla\phi| = 0 \tag{9}$$

$$\phi(x, t = 0) \quad given \tag{10}$$

Now consider a speed function of the form $1 - \epsilon\kappa$, where ϵ is a constant. An evolution equation for the curvature κ, see [35], is given by

$$\kappa_t = \epsilon\kappa_{\alpha\alpha} + \epsilon\kappa^3 - \kappa^2 \tag{11}$$

where we have taken the second derivative of the curvature κ with respect to arclength α. This is a reaction-diffusion equation; the drive toward singularities due to the reaction term $(\epsilon\kappa^3 - \kappa^2)$ is balanced by the

(a) Original image with Gaussian Noise

(b) Reconstructed Min/Max Flow

Figure 6: Continuous Gaussian Noise added to Image

smoothing effect of the diffusion term ($\epsilon\kappa_{\alpha\alpha}$). Indeed, with $\epsilon = 0$, we have a pure reaction equation $\kappa_t = -\kappa^2$. In this case, the solution is $\kappa(s,t) = \kappa(s,0)/(1+t\kappa(s,0))$, which is singular in finite t if the initial curvature is anywhere negative. Thus, corners can form in the moving curve when $\epsilon = 0$.

For $\epsilon = 0$, the front develops a sharp corner in finite time as discussed above. In general, it is not clear how to construct the normal at the corner and continue the evolution, since the derivative is not defined there. One possibility is the "swallowtail" solution formed by letting the front pass through itself. However, from a geometrical argument it seems clear that the front at time t should consist of only the set of all points located a distance t from the initial curve. (This is known as the Huyghens principle construction, see [35]). Roughly speaking, we want to remove the "tail" from the "swallowtail". Another way to characterize this weak solution is through the following "entropy condition" posed by Sethian (see [35]): If the front is viewed as a burning flame, then *once a particle is burnt it stays burnt.* Careful adherence to this stipulation produces the Huyghens principle construction. Furthermore, this physically reasonable weak solution is the formal limit of the smooth solutions $\epsilon > 0$ as the curvature term vanishes, (see [35]). Extensive discussion of the role of shocks and rarefactions in propagating fronts may be found in [34].

Motivated by the above discussion, in [25] this formulation was applied to shape recovery. First, we split the influence of the speed function into two parts $F = F_A + F_G$. The term F_A is the advection term causing the front to uniformly expand or contract with speed F_A depending on its sign and is analogous to the inflation force defined in [13]. The second term F_G, is the part which depends on the geometry of the front, such as its local curvature. This (diffusion) term smooths out the high curvature regions of the front and has the same regularizing effect on the front as the internal deformation energy term in thin-plate-membrane splines [19].

Our goal now is to define a speed function from the image data that can be applied to this motion to act as a halting criterion. We multiply the above speed function by the term:

$$k_I(x,y) = \frac{1}{1+\mid \nabla G_\sigma * I(x,y) \mid}, \tag{12}$$

where the expression $G_\sigma * I$ denotes the image convolved with a Gaussian smoothing filter whose characteristic width is σ. In fact, one must be a bit careful with Eqn.12, since it technically has meaning only on the zero level set of ϕ; issues about extension velocities and fast narrow band techniques may be found in [25].

As a demonstration, we show the recovery of human thighs along with the thigh bone in a single calculation. Figure 7(a) depicts a single slice from a CT (computed tomography) image of human thighs. This is an example of an image containing several shapes of interest; we recover all of them by exploiting the topological adaptability of our scheme. After initialization in figure 7(a), the front which consists of two separate parts is made to propagate in the normal direction with speed $F = 1 - .01\kappa$. We employ the narrow-band algorithm with a band width of $\delta = 0.06$ to move the front. It can be seen that in subsequent frames the front evolves into the shapes, wraps itself around the bone (see Fig. 7(d)), splits in Fig. 7(e), and finally reconstructs both thighs and the outline of bones inside (see Fig. 7(f)). Calculations were carried out on a 128×128 grid and a time step $\Delta t = 0.0005$ was used.

5 Comparison with Other Techniques and Coupling

In this section, we examine the performance of our min/max flow against some standard norms. We then follow by detailing the mechanism that connects our min/max flow to our shape recovery techniques, and then follow with extensions of our basic min/max flow and shape recovery technique to related work.

5.1 Edge Detection

We begin with an examination of the edge localization capabilities of our min/max scheme. It is a commom practice to convolve a given image with a smoothing filter before edge detection. This will prevent the detection of false edges due to noise. As an example consider the CT image shown in Fig. 8(a). In Fig. 8(b), we show the corresponding edge map obtained by marking the points at which the second derivative of the image changes sign; it is clear from this figure that the edge map is corrupted with too many noise-edges. Next, we run the isotropic heat equation (same as the Gaussian smoothing filter) before detecting edges and show the result in Fig. 8(c). As noted before, smoothing an image with isotropic heat equation compromises region boundary definition and therefore is unacceptable. On the other hand, smoothing with curvature flow, i.e. speed $F = \kappa$ in Eqn. 6 retains more of the region definition (see Fig. 8(d)) but some regions merge and with time shrink and disappear. Finally, in Fig. 8(e) we show edge detection after running our min/max scheme on the image and from the Fig. 8(f), it is clear that the above description does not deteriorate with time. Note that Figs. 8(d) and 8(e) were produced by running the corresponding diffusion equations for the

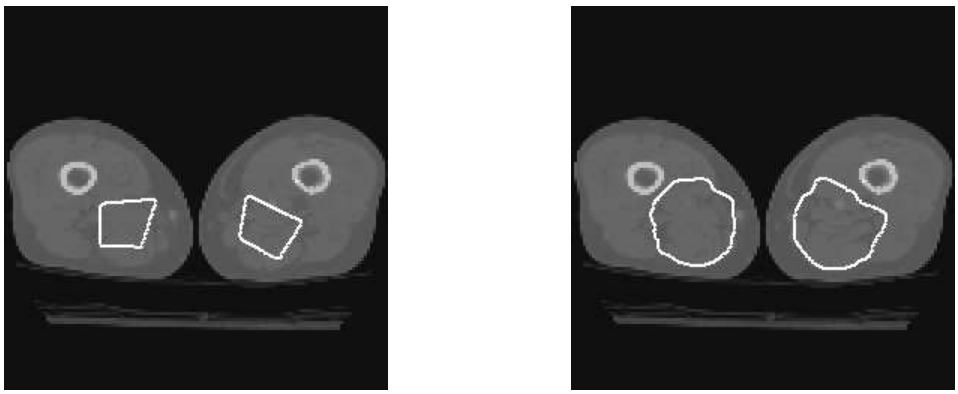

(a) $t = 0.0000$

(b) $t = 0.2000$

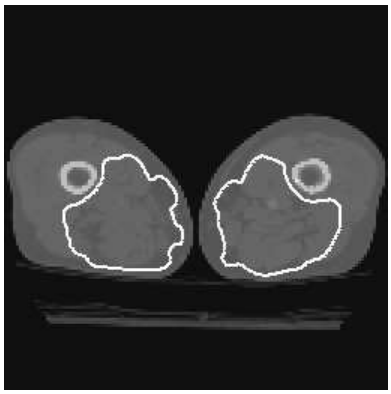

(c) $t = 0.4000$

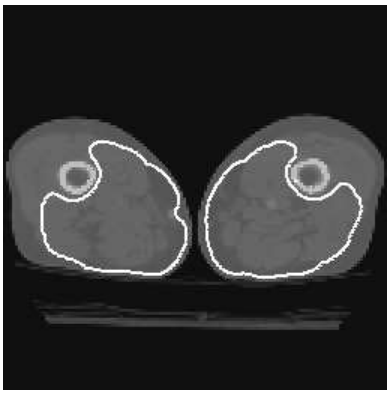

(d) $t = 0.6000$

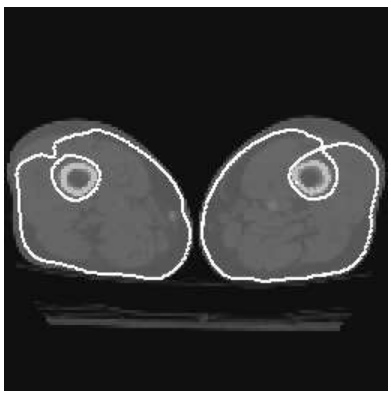

(e) $t = 1.0000$

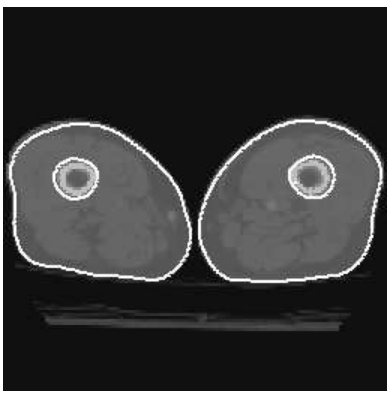

(f) $t = 1.6000$

Figure 7: Reconstruction of human thighs and the thigh bones in a single calculation: a time step of $\Delta t = 0.0005$ was employed on a 128×128 grid. The narrow-band algorithm was used with a band width of $\delta = 0.06$.

same number of time steps.

5.2 Knowledge of Noise; Comparison with Wiener Filters

The basic approach of our min/max flow is to make no assumptions about the type, distribution or qualities of the noise in the image. Thus, our approach is independent of any knowledge about the noise. It is interesting to compare our results using our min/max scheme on Gaussian noise with those obtained using a more traditional approach such as a Wiener filter. Figure 6(a) depicts an image corrupted with Gaussian noise with zero mean and Fig. 9 is the result of restoring it using a Wiener filter. The result of applying our min/max scheme on the same image is shown in Fig. 6(b). Here we have used the scheme in Eqn. 8 with the coupling $\min / \max(\kappa/|\nabla\phi|, 0)$. For best results, the iterative scheme has been stopped before steady-state is achieved.

5.3 Coupling of Min/Max Scheme to Shape Recovery

The shape recovery scheme presented in a previous section rests on convolving the image with a Gaussian smoothing filter of a given characteristic width; see Eqn. 12. As mentioned above, Gaussian smoothing filter does not preserve edges. Moreover, the propagation of our shape as it evolves towards the boundary slowed by variations in the image intensity which do not correspond to the desired boundary, but still slow the evolution. However, if we use our image enhancement schemes given by the min/max flow, edges are sharpened, and intraregions away from the boundaries are significantly smoothed as noise is removed and regions are made piecewise smooth. Thus, by coupling the two, we can provide very rapid evolution of the shape recovery algorithm towards a well-defined edge. Thus, we rewrite Eqn. 12 as

$$k_I(x, y) = \frac{1}{1 + | \nabla I_{min/max}(x, y) |}, \tag{13}$$

where $I_{min/max}$ is the image enhanced using our min/max flow. We present some examples of this in the following section.

5.4 Extensions to Related Schemes

Previous work on partial differential equation/level set schemes for image processing may be easily incorporated into our framework; in short, the curvature flow is replaced by our min/max flow. We point out a few couplings in particular:

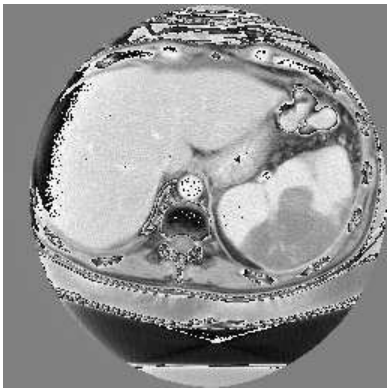

(a) CT Image

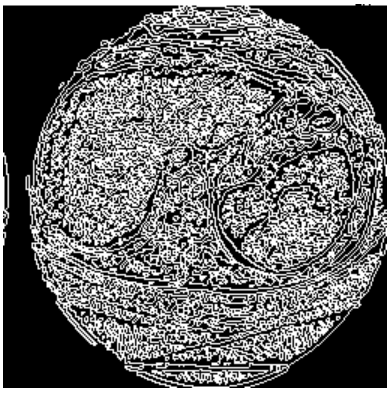

(b) Noisy edges

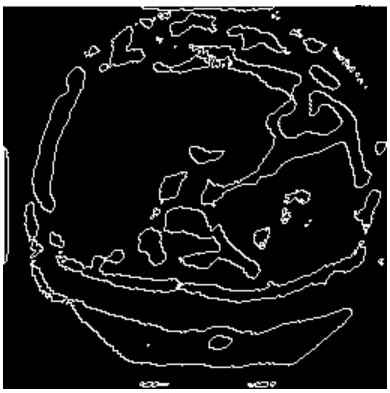

(c) Gaussian Filter

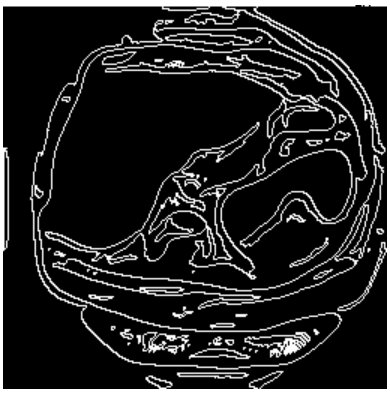

(d) Curvature Flow

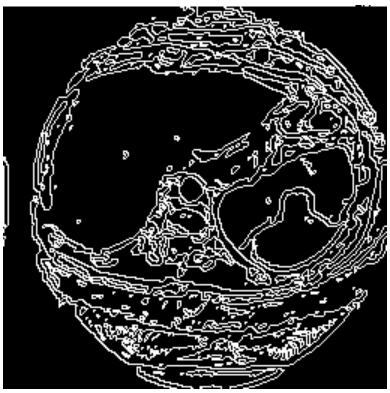

(e) Min/Max

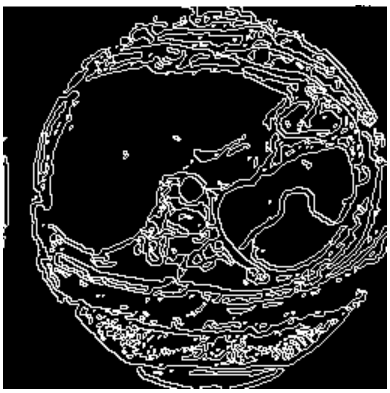

(f) Min/Max($T \to \infty$)

Figure 8: Edge detection after applying various smoothing operators like the Gaussian filter, curvature flow, and the min/max flow.

(a) Wiener filtered

Figure 9: Wiener filtered restoration of the image in Fig. 6(a).

- Image sharpening algorithms based on shock filters, as in [27, 4] may be coupled to our min/max flow.
- The rate of smoothing is sometimes made to vary inversely with the gradient magnitude [30]. If such an effect is desired in our setting, one merely replaces the curvature κ in our flow $\min / \max(\kappa, 0)$ by $\kappa/|\nabla\phi|$.
- The affine invariant flow $\kappa^{1/3}$ [32] can also be modified by using the $\min / \max(\kappa^{1/3}, 0)$.

6 Results

In this section, we present some results of the enhancement of medical images and ensuing shape recovery using the level set methodology presented above.

6.1 Enhancement of Medical Images

We begin in Fig. 10 by enhancing a series of medical images. Here, no noise is artificially added, instead our goal is to enhance certain features within the given images.

(a) Original image

(b) Min/Max:Final

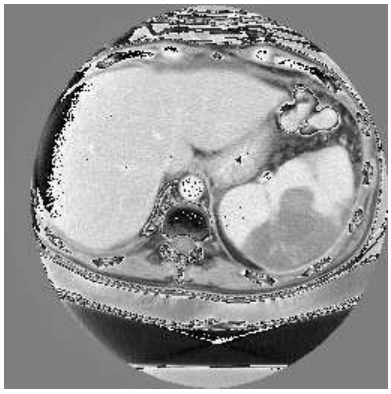

(c) Original image

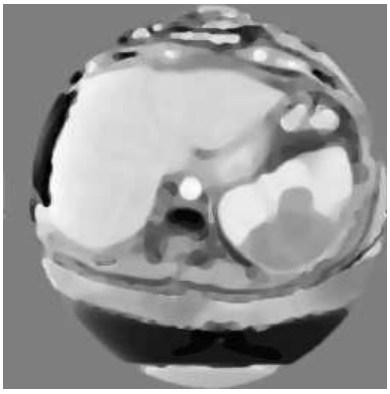

(d) Min/Max:Final

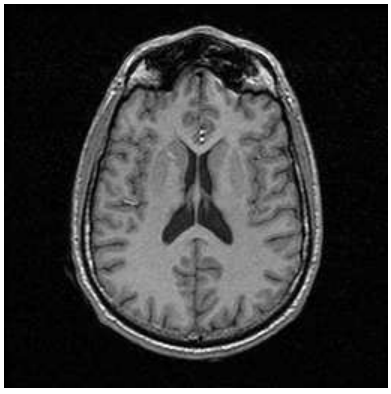

(e) Original image

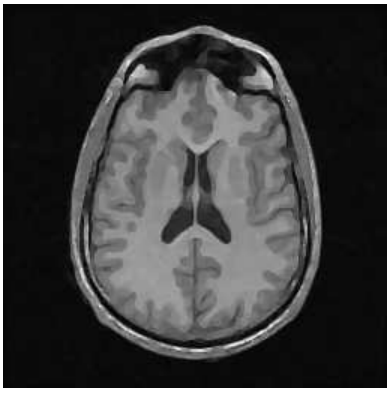

(f) Min/Max:Final

Figure 10: Min/Max Flow with Selective Smoothing

6.2 Extraction of Shapes from Medical Data

Lastly, we present some shape recovery results obtained by using the image-based speed given in Eqn. 13. The regions of interest are first "tagged" using a mouse-based control, thus defining the initial state as depicted in the left column in Fig. 11. These initial shapes grow out and eventually recover the shapes, cross sections of cardiac chamber in Fig 11(b) and the liver in Figs. 11(d) & 11(f).

Acknowledgements: All calculations were performed at the University of California at Berkeley and the Lawrence Berkeley National Laboratory. We thank Gilbert Chang for medical data in Fig. 11.

References

[1] D. Adalsteinsson and J. A. Sethian, "A fast level set method for propagating interfaces," *J. Comp. Phys.*, Vol. 118(2), pp. 269–277, May 1995.

[2] D. Adalsteinsson and J. A. Sethian, "A unified level set approach to etching, deposition and lithography: I, II, and III." I, II: to appear, *J. Comp. Phys.*, 1995; III: under preparation.

[3] L. Alvarez, P. L. Lions, and J. M. Morel, "Image selective smoothing and edge detection by nonlinear diffusion. II," *SIAM Journal on Numerical Analysis*, Vol. 29(3), pp. 845–866, 1992.

[4] L. Alvarez and L. Mazorra, "Signal and image restoration using shock filters and anisotropic diffusion," *SIAM J. Numer. Anal.*, Vol. 31, No. 2, pp. 590–605, April 1994.

[5] R. Bajcsy and F. Solina, "Three dimensional object representation revisited," in *Proceedings of First International Conference on Computer Vision*, pp. 231–240, London, England, 1987.

[6] T. O. Binford, "Visual Perception by computer," invited talk, *IEEE Systems and Control Conference*, Miami, Florida.

[7] A. Blake and A. Zisserman, *Visual Reconstruction*, MIT Press, Cambridge, MA.

[8] J. Canny, "A computational approach to edge detection," *IEEE Trans. Pattern Analysis and Machine Intelligence*, Vol. PAMI-8, pp. 679–698, 1986.

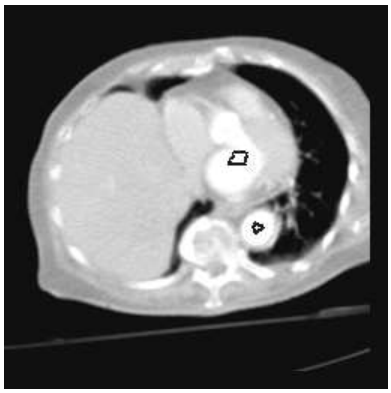

(a) Initialization

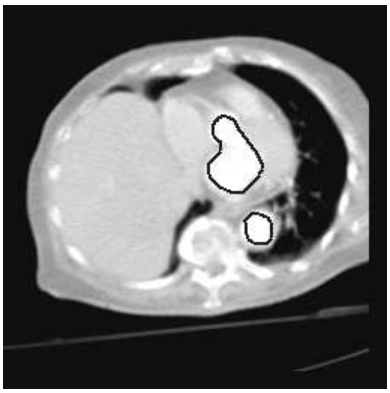

(b) Extracted Shapes

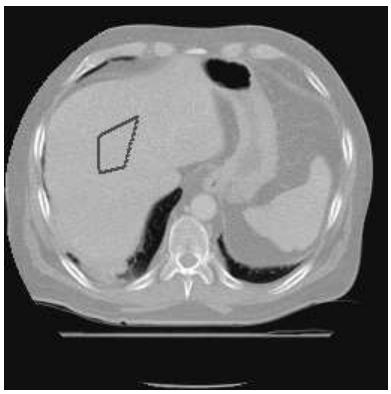

(c) Initialization

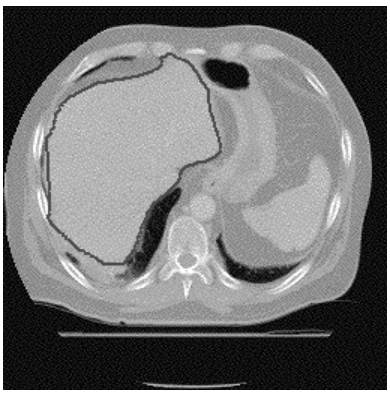

(d) Extracted Shape

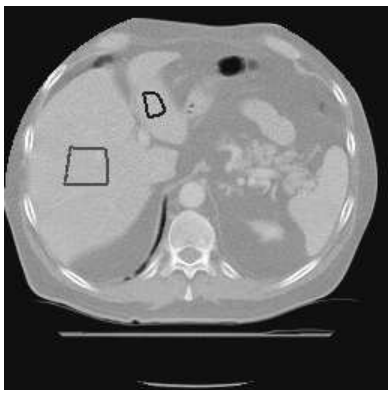

(e) Initialization

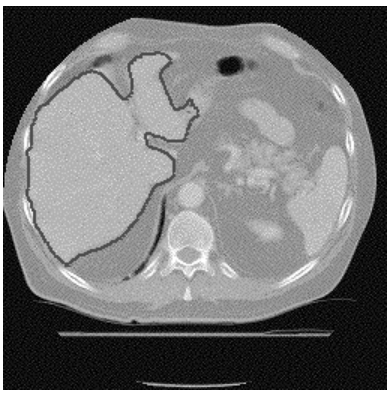

(f) Extracted Shape

Figure 11: Shape extraction from medical data using the speed term from Eqn. 13.

[9] V. Caselles, F. Catté, T. Coll, and F. Dibos, "A geometric model for active contours in image processing," *Numerische Mathematik*, Vol. 66(1), pp. 1–32, 1993.

[10] V. Caselles, R. Kimmel, and G. Sapiro, "Geodesic snakes," *Proc. of ICCV*, MIT, Cambridge MA, June 1995.

[11] D. L. Chopp, "Computing minimal surfaces via level set curvature flow," *Journal of Computational Physics*, Vol. 106, pp. 77–91, 1993.

[12] D. L. Chopp and J. A. Sethian, "Flow under curvature: singularity formation, minimal surfaces, and geodesics," *Jour. Exper. Math.*, Vol. 2(4), pp. 235–255, 1993.

[13] L. D. Cohen, "On active contour models and balloons," *Computer Vision, Graphics, and Image Processing*, Vol. 53, No. 2, pp. 211–218, March 1991.

[14] D. F. Elliot and K. R. Rao, *Fast transforms: Algorithms, Analyses, Applications*, Academic Press, New York, 1982.

[15] M. Gage, "Curve shortening makes convex curves circular," *Inventiones Mathematica*, Vol. 76, pp. 357, 1984.

[16] R. C. Gonzalez and P. Wintz, *Digital Image Processing (2nd Ed.)*, Addison-Wesley, 1987.

[17] M. Grayson, "The heat equation shrinks embedded plane curves to round points," *J. Diff. Geom.*, Vol. 26, pp. 285–314, 1987.

[18] A. K. Jain, *Fundamentals of digital image processing*, Englewood Cliffs, NJ : Prentice Hall, 1989.

[19] M. Kass, A. Witkin, and D. Terzopoulos, "Snakes: Active contour models," *International Journal of Computer Vision*, pp. 321–331, 1988.

[20] R. Malladi and J. A. Sethian, "Image processing via level set curvature flow," to appear *Proc. Natl. Acad. of Sci., USA*, 1995.

[21] R. Malladi and J. A. Sethian, "Image Processing: Flows under Min/Max curvature and mean curvature," submitted to *Graphical Models and Image Processing*, July 1995.

[22] R. Malladi and J. A. Sethian, "A unified approach for shape segmentation, representation, and recognition," Report LBL-36069, Lawrence Berkeley Laboratory, University of California, Berkeley, August 1994.

[23] R. Malladi, D. Adalsteinsson, and J. A. Sethian, "Fast method for 3D shape recovery using level sets," under preparation.

[24] R. Malladi, J. A. Sethian, and B. C. Vemuri, "Evolutionary fronts for topology-independent shape modeling and recovery," in *Proceedings of Third European Conference on Computer Vision*, LNCS Vol. 800, pp. 3–13, Stockholm, Sweden, May 1994.

[25] R. Malladi, J. A. Sethian, and B. C. Vemuri, "Shape modeling with front propagation: A level set approach," *IEEE Trans. on Pattern Analysis and Machine Intelligence*, Vol. 17(2), pp. 158–175, Feb. 1995.

[26] D. Marr and E. Hildreth, "A theory of edge detection," *Proc. of Royal Soc. (London)*, Vol. B207, pp. 187–217, 1980.

[27] S. Osher and L. I. Rudin, "Feature-oriented image enhancement using shock filters," *SIAM J. Num. Anal.*, Vol. 27, pp. 919–940, 1990.

[28] S. Osher and J. A. Sethian, "Fronts propagating with curvature dependent speed: Algorithms based on Hamilton-Jacobi formulation," *Journal of Computational Physics*, Vol. 79, pp. 12-49, 1988.

[29] P. Perona and J. Malik, "Scale-space and edge detection using anisotropic diffusion," *IEEE Trans. Pattern Analysis and Machine Intelligence*, Vol. 12(7), pp. 629–639, July 1990.

[30] L. Rudin, S. Osher, and E. Fatemi, "Nonlinear total variation based noise removal algorithms," *Modelisations Matematiques pour le traitement d'images*, INRIA, pp. 149–179, 1992.

[31] W. B. Ruskai *et al.*, *Wavelets and their applications*, Jones and Barlett Publishers, Boston, MA 1992.

[32] G. Sapiro and A. Tannenbaum, "Image smoothing based on affine invariant flow," *Proc. of the Conference on Information Sciences and Systems*, Johns Hopkins University, March 1993.

[33] G. Sapiro and A. Tannenbaum, "Area and length preserving geometric invariant scale-spaces," *Proc. of Third European Conference on Computer Vision*, LNCS Vol. 801, pp. 449–458, Stockholm, Sweden, May 1994.

[34] J. A. Sethian, "An analysis of flame propagation," Ph.D. Dissertation, Mathematics, University of California, Berkeley, 1982.

[35] J. A. Sethian, "Curvature and the evolution of fronts," *Commun. in Mathematical Physics*, Vol. 101, pp. 487–499, 1985.

[36] J. A. Sethian, "Numerical algorithms for propagating interfaces: Hamilton-Jacobi equations and conservation laws," *Journal of Differential Geometry*, Vol. 31, pp. 131–161, 1990.

[37] J. A. Sethian, "Curvature flow and entropy conditions applied to grid generation," *Journal of Computational Physics*, Vol. 115, No. 2, pp. 440–454, 1994.

[38] D. Terzopoulos, "Regularization of inverse visual problems involving discontinuities," *IEEE Trans. on Pattern Analysis and Machine Intelligence*, Vol. PAMI 8, No. 2, pp. 413–424, 1986.

[39] D. Terzopoulos, A. Witkin, and M. Kass, "Constraints on deformable models: Recovering 3D shape and nonrigid motion," *Artificial Intelligence*, 36, pp. 91–123, 1988.

[40] C. Rhee, L. Talbot, and J. A. Sethian, "Dynamical study of a premixed V flame," to appear, *Jour. Fluid Mech.*, 1995.

[41] B. C. Vemuri and R. Malladi, "Constructing intrinsic parameters with active models for invariant surface reconstruction," *IEEE Trans. on PAMI*, Vol. 15, No. 7, pp. 668–681, July 1993.

[42] J. Zhu and J. A. Sethian, "Projection methods coupled to level set interface techniques," *J. Comp. Phys.*, Vol. 102, pp.128-138, 1992.